Ionic Disruption of the Liquid−Liquid Interface

Eric S. Shamay and Geraldine L. Richmond*

Department of Chemistry, University of Oregon, 210 Willamette Hall, 1253 University Ave., Eugene, Oregon 97405

Received: March 15, 2010; Revised Manuscript Received: May 6, 2010

The interface formed between an aqueous salt solution and a hydrophobic liquid has been investigated using molecular dynamics simulations. The salt solutions of NaCl, $NaNO_3$, and Na_2SO_4 have been studied to determine their presence and distribution in the interfacial region and their effect on interfacial water molecules. Density and orientation profiles reveal the formation of ionic double layers with widths that vary with the respective anions' surface affinities and effects on the geometry of interfacial water molecules. The NO_3^- anion shows enhanced surface concentration above that of the bulk aqueous phase, whereas the Cl^- and SO_4^{2-} anions exhibit similar characteristics as are found for corresponding air−water interfaces. Sum frequency spectra were calculated for the OH vibrational modes of water to show the effect of the various ions on the hydrogen-bonding network strength of interfacial water. These calculated spectra show good agreement with the conclusions and observations of our recent spectroscopic experimental study, while providing important new detailed insights into interfacial behavior to augment that study.

1. Introduction

The most important biological and environmental processes depend on the nature of interfacial water molecules and dissolved ions in boundary layers. Only in recent years, and through the development of surface-specific experimental[1−3] and computational[4−6] analytical techniques, have we been able to begin understanding this complex environment comprised of interfacial water and ions. Over this time the field has advanced from studying simple water systems in vacuum and in air to studying more complex interfaces such as aqueous solutions near a hydrophobic surface that are responsible for such important processes as ion transport, liquid−liquid extraction, drug delivery, and environmental remediation.

The computational studies presented herein have been conducted to gain a more precise molecular-level picture of how ions affect waters within a liquid−liquid interface. Molecular dynamics (MD) simulations allow us to look at the specific ion and water locations, geometries, and bonding environments within the interface region, unlike experimental techniques currently used for similar surface studies. Consequently, the work presented here is compared to conclusions from a recent experimental study that showed how ions affect the interfacial region between an aqueous ionic solution and a hydrophobic organic liquid.[7] Classical molecular dynamics simulations have been performed to analyze the interface formed between various aqueous salt solutions and the organic liquid carbon tetrachloride (CCl_4). Analyses were conducted to contrast the behavior of different aqueous salt solutions as well as for comparison with previous computational efforts.[8−13] Three salt solutions were simulated containing NaCl, $NaNO_3$, Na_2SO_4. These were chosen to show the effects of both atomic and molecular as well as monovalent and divalent anions on the interfacial environment. The simulation data has been used here to extract ionic and molecular density data across organic interfaces, information about water orientation near the interfaces, and simulated SFG spectra.

1.1. Density Profiles. Density histograms of simulated interfaces have been used in previous publications to show ionic and molecular distribution behavior in various systems.[9,11,13−18] In this work the density profile of water throughout the interface is fit to a hyperbolic tangent function[17,19] as shown here:

$$\rho(z) = \frac{1}{2}(\rho_1 + \rho_2) - \frac{1}{2}(\rho_1 - \rho_2)\tanh\left(\frac{z - z_0}{d}\right) \quad (1)$$

Equation 1 relates the interfacial density, ρ, as a function of position, z, along a given system reference axis, to the densities of the phases, ρ_1 and ρ_2, on either side of the Gibb's dividing surface (GDS), z_0. The interfacial width, d, is related to the "90−10" thickness that is often reported by $t_{90-10} = 2.197d$.

These measures of interfacial thickness provide a means of comparing the depths to which the water phase is affected by ions located at the interface. The density distributions of the salts depict concentration and depletion phenomena throughout the interfacial region and also serve to illustrate ionic surface affinity within this region. Previous work has been performed on the air−H_2O interface with ions of different levels of interfacial affinity, with the more polar ions being the most interfacially active.[3,18,20−25] We present the density distribution results for the neat CCl_4−H_2O and salt solutions adjacent to an organic CCl_4 phase.

1.2. Molecular Orientation. Several methods have been used previously to show molecular orientation profiles of water molecules throughout simulated interfacial regions.[4,8,9,17,26−30] Studies have utilized various internal coordinate definitions and a number of angle definitions, orientational order parameters, and probability distributions to relate molecular, or averaged, orientations. In this work, we have chosen to compute the orientation of water using two vectors that intuitively describe the orientation in space, given the locations of the three atoms

* To whom correspondence should be addressed. E-mail: richmond@uoregon.edu.

10.1021/jp1023668
Published on Web 07/06/2010

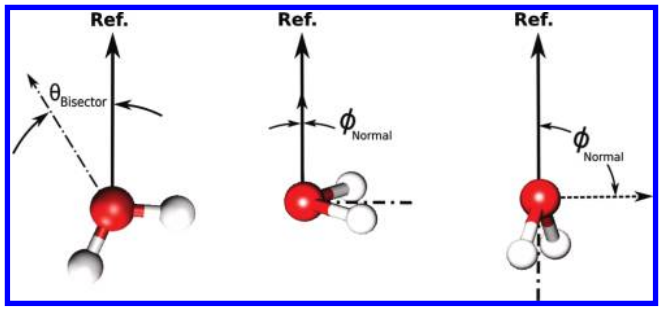

Figure 1. Angles used to define the molecular orientation. The system reference (Ref.) axis is that which is perpendicular to the plane of the aqueous−organic interface and points out from the aqueous phase into the organic one. The molecular bisector vector points from the hydrogen end of the water to the oxygen end and orients along the axis of symmetry. The angle it forms with the reference axis is either aligned or antialigned such that $-1 \leq \cos\theta \leq 1$. The angle formed between the vector normal to the molecular plane (formed by the three water atoms) and the reference axis orients the "twist" of the molecule such that $0 \leq \cos\phi \leq 1$, where the water molecular plane is either laying flat on the interface ($\cos\phi = 1$), or the water is perpendicular to the interface ($\cos\phi = 0$).

comprising the molecule. The molecular bisector, a vector that points along the axis of symmetry of the water molecule from the hydrogen end to the oxygen, provides directional orientation similar to the water molecule's dipole. A second vector, which is referred to here as the molecular normal vector, is established as the vector pointing normal to the plane formed by the three atoms of the water molecule and establishes its planar "tilt". Analyzing the angle made between these two vectors and a given space-fixed reference axis (herein defined as the long-axis of the simulation cells, oriented perpendicular to the interfacial plane and pointing out of the aqueous phase) is a means of finding the orientation of waters within these simulated systems as illustrated in Figure 1. The angle formed between the molecular bisector and the reference axis will hereafter be referred to as θ, and the angle between the reference axis and the molecular normal vector as ϕ. The analysis in this work reports the cosines of these two angles, and because of the symmetry of the water molecule, where the hydrogens are not uniquely identified, the cosines of the two angles are limited as follows: $-1 \leq \cos\theta \leq 1$ and $0 \leq \cos\phi \leq 1$. We report the orientation profiles of θ and ϕ as functions of the distance from the GDS of the interface, as found from the fitting in our density profile analyses.

1.3. Computational SFG. A difficult challenge for experimental surface studies is in understanding the vibrational spectroscopy of liquid water. Hydrogen bonding between water molecules causes inter- and intramolecular couplings that lead to broad spectral envelopes, each containing a distribution of water-bonded species. Simulations provide the analytical capacity to relate the broad line shapes, and the often difficultly assessed impact of hydrogen bonding as a function of OH vibrational frequency, to microscopic geometries, forces, and environments. In this work, we compute the SFG spectra of the interface between the salt solutions and an organic phase to compare with the experimental results of similar systems.[7]

The computational method used in this work is based on that of Morita and Hynes[31] as outlined in a previous study by this group utilizing the same technique.[32] The computational SFG technique has been improved in more recent studies by Morita et al.[33,34] and with other enhanced water models. The technique used in this work matches qualitatively the experimental spectra to a sufficient degree such that we may draw qualified conclusions about line shape and intensity.

TABLE 1: Aqueous Molecule and Ion Numbers[a]

system	H_2O	cation	anion
neat water	1800	0	0
NaCl	1759	40	40
$NaNO_3$	1732	40	40
Na_2 SO_4	1740	86	43

[a] Listed are the populations of each component for the four simulated aqueous phases. All systems were simulated at near 1.2 M salt concentrations.

2. Computational Method

The molecular dynamics methods used in this work are similar to those from our previous computational efforts with some modifications described below.[8,9,11] Simulations were carried out using the Amber 9 software package. The polarizable ion model parameters are taken from previous works on similar systems.[14,26,35−37] The polarizable POL3 model was used for water molecules.[38] Fully polarizable models have been used in previous interface simulation studies because they are known to more accurately reproduce interfacial structure and free energy profiles.[27,39−42]

A total of four systems were simulated consisting of aqueous salt and CCl_4 phases. A slab geometry was used to produce two interface regions within each simulation cell.[8] The results of the analyses performed herein on each simulated system made use of the natural symmetry of the two interfaces by averaging the results from the two surfaces. The organic region was formed in a box 30 Å on a side with 169 CCl_4 molecules to reproduce a standard temperature density of 1.59 g/mL. The aqueous region was formed in a box $30 \times 30 \times 60$ Å^3, with the long axis perpendicular to the interfaces. The number of water molecules and ions varied for each system in order to reproduce a concentration of 1.2 M. The specific populations of each molecule are listed in Table 1. The organic and aqueous boxes were then joined to form a system 90 Å long with interface areas of 30×30 Å^2.

The water, salts, and CCl_4 were each randomly packed into their respective boxes with a minimum packing distance of 2.4 Å. After joining the aqueous and organic phases and forming the two interfaces, the total system was energy minimized using a conjugate gradient method. Following minimization, the system was equilibrated at a constant temperature of 298 K with weak coupling to a heat bath for a period of 10 ns, using a simulation time step of 1.0 fs. A nonbonded potential cutoff of 9.0 Å was used. Following equilibration the system was simulated with the same parameters for a further 10 ns with atomic position data recorded every 50 fs. This resulted in a total of 200 000 snapshots that were used in the data analysis.

3. Component Densities

The component density profiles of each system were calculated to study the effects of added salts on water's density profile and to find any deviations in the behavior of water from the neat CCl_4−H_2O system. The water density profile of each system was fitted to a hyperbolic tangent function (eq 1). The resulting profiles are plotted in Figure 2. The profiles were centered about the GDS locations, z_0, at 0.0 Å, and all line shapes are plotted as distances to the GDS. Each interfacial width, d, is designated as a highlighted blue region of width d centered about z_0. The widths of the interfacial regions for the neat CCl_4−H_2O (A), NaCl (B), $NaNO_3$ (C), and Na_2SO_4 (D) systems are 2.16, 2.62, 2.20, 3.69 Å, respectively. In each of the salt solutions, the anion density profile shows higher density

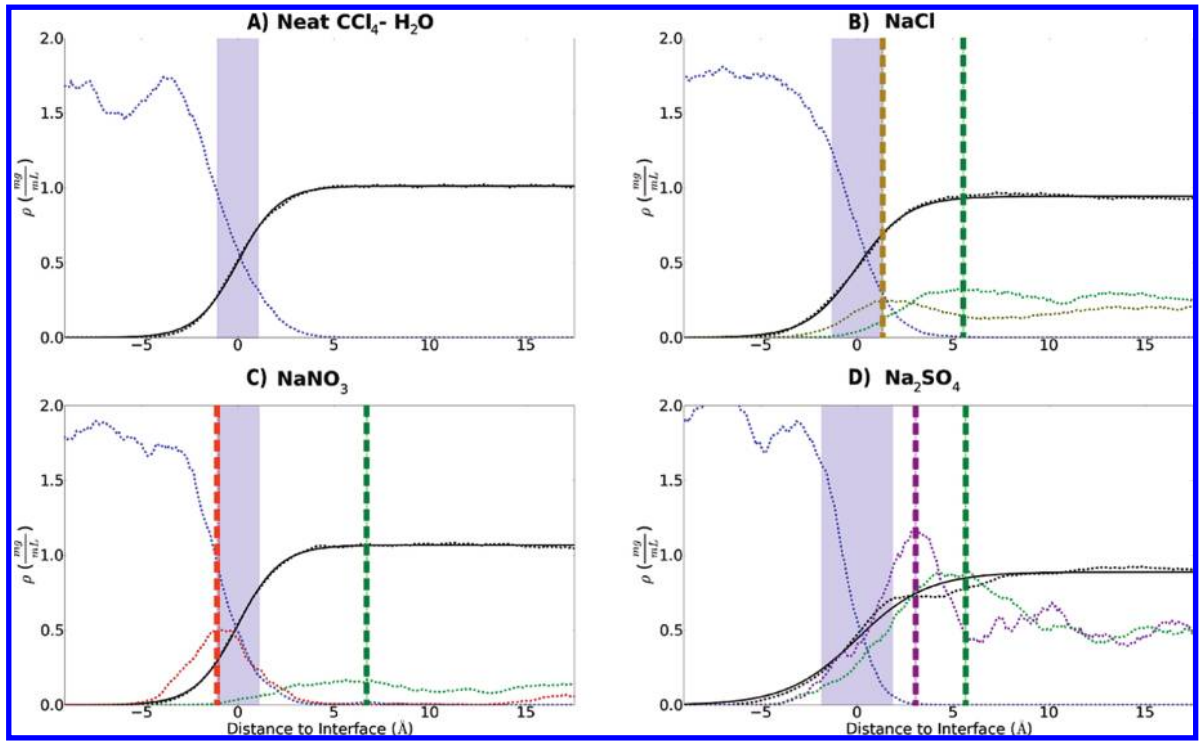

Figure 2. Aqueous salt solution (1.2 M) and CCl_4 surface density profiles. (A) Neat CCl_4-H_2O, (B) NaCl, (C) $NaNO_3$, and (D) Na_2SO_4 aqueous solution densities are plotted with the water-oxygen density (dashed black) and the corresponding fitted line shape (solid black). The CCl_4 (dashed blue), Na^+ cation (dashed green, scaled 10×), and respective anion (scaled 5×) densities are also shown for each system. The maxima of the ionic components are marked with dashed vertical lines of the same colors.

TABLE 2: Aqueous Salt System Density Parameters[a]

system	d	anion (Å)	cation (Å)	anion−cation distance (Å)
neat H_2O	2.16	−	−	−
NaCl	2.62	1.33	5.53	4.20
$NaNO_3$	2.20	−0.99	6.71	7.70
Na_2SO_4	3.69	3.04	5.64	2.60

[a] Interfacial widths, d, and the locations of the maxima of the density profiles for each ionic component are listed for the simulated salt systems. The relative distances between the anion and cation density peak locations are listed to show how the different anions affect the relative location of their cationic counterions.

near the interface, appearing as a peak in the density profile. These anion enhancements all occur closer to the interface than the corresponding countercation density enhancement. Various parameters of interest such as the interfacial thicknesses, ionic enhancement locations (taken to be the location of the maxima in the ion profiles), and relative distances between the peaks of the ion profiles are collected in Table 2. Unlike experimental surface studies, our simulation results provide a full microscopic view of ion location and stratification within the interfacial region.

The oscillations in the surface density profiles of water and the adjoining organic CCl_4 liquid phase have been noted previously and attributed to thermal capillary waves on a larger length scale than the simulated system size.[43] The same work also made note that the interfacial thickness is size-dependent on the interfacial surface area. Increasing the surface area dimensions should therefore cause a proportional increase in the interfacial width. As a consequence, care must be taken when making quantitative comparisons between widths and locations found in differing simulation studies. However, relative width ordering between similarly sized systems should remain, as shown in two separate works on the CCl_4-H_2O surface.[9,43]

In comparing the three salt solutions studied here, any differences in these systems are the result of the anion because the same cation was used in each system. NaCl is the simplest of the three salts with a monatomic and monovalent anion. The peak of the anion density profile is within the aqueous phase (i.e., it is found on the aqueous side of the interfacial width). The location of the cation density peak is, as mentioned above, deeper in the aqueous phase than the anion by over 4 Å. This layering of ions within the aqueous phase is attributed to the break in the isotropy of the field of the bulk region upon introduction of the organic phase. From our studies it is clear that polarizable monovalent anions move toward the interface and effectively screen the induced field from the organic phase. The counterions then are drawn toward the negative charge built up by the anions to create the second ion density peak deeper in the aqueous phase. The overall shape of the water profile in the NaCl system is relatively unaffected (compared to the reference CCl_4-H_2O system, Figure 2a) by the presence of the ions. The width of the interface is slightly increased above that of the reference system. The behavior at a CCl_4-H_2O surface is markedly similar to that of NaCl at the air$-H_2O$ interface, as determined by a previous MD study.[4]

It is important to note from our density calculations that ions that increase the interfacial width at the CCl_4-H_2O interface correspond to ions that result in an enhancement of the SFG signal from interfacial water. As discussed later, our SFG calculations show excellent agreement with experimental results that also show this enhancement for such ions. Also, we find those ions that are best known to enhance the strength of hydrogen bonding (i.e., SO_4^{2-}) produce wider interfaces with greater water penetration into the CCl_4 phase.

The $NaNO_3$ system introduces the monovalent, polyatomic nitrate anion. In our simulation we find a strong surface density enhancement of the nitrate anion, as shown in Figure 2c. The

nitrate density peak is located the furthest out from the aqueous phase of the three salt systems. The location of the sodium cation peak in this system is a significant distance further into the bulk water relative to the anion than in either the NaCl or Na_2SO_4 systems. The increase in ion-pair distance is likely the result of strong screening of the interfacial field by the surface-active anion and the solvating waters around it. The interfacial width of the $NaNO_3$ system is the narrowest relative to the other salts in this study. It is likely that slight reorientation of the surface waters near CCl_4 enhance the solvation of the NO_3^- in the plane of the interface and establish a much more hydrated region for the anion to adsorb. Water reorientation is more fully described later in this work. The subsurface waters then continue to screen the charge of the surface-active NO_3^- and decrease the Coulombic force pulling the cation closer to the surface.

The widest interface is that of the Na_2 SO_4 solution, indicating that the SO_4^{2-} anions act to increase the number of interfacial water molecules on both sides of the GDS, consistent with the highly solvated nature of SO_4^{2-} and its larger size. SO_4^{2-} density enhancement (the peak of the anion density profile) is furthest into the aqueous bulk of the three anions simulated. The calculations suggest that the divalent and highly polarizable nature of the SO_4^{2-} anion attracts its counterion closest, leading to the narrowest subsurface ionic double layer. This attraction is likely Coulombic. Although the greatest anionic concentration enhancement is further into the bulk water region, seemingly outside the region designated by the interfacial width, the water interfacial width is still greatly enhanced. This is in agreement with the experimental Na_2SO_4 SFG studies, where sulfate ion leads to an enhanced SFG signal throughout the bonded OH stretch region, consistent with a larger interfacial width.[7]

The results of these and related simulations of ions at liquid−liquid interfaces, and the recent experimental results of similar systems, demonstrate that some ions behave at the CCl_4−H_2O interface very differently than what has been calculated and observed at air−water interfaces.[44−46] The most striking example is that of the polyatomic nitrate ion, which has been investigated at the air−H_2O interface by computer simulation,[26,47] SHG and SFG spectroscopies,[48−50] and depth-resolved X-ray photoemission spectroscopy.[51] In contrast to what is observed here and in the related experimental SFG studies of the CCl_4−H_2O interface, where nitrate ion shows an enhanced presence in the interfacial region, at the air−H_2O interface the nitrate ion shows no greater affinity for the surface than the bulk water. The large planar geometry of the NO_3^- anion and its low charge appear to repel it from the air−H_2O surface, where it encounters a reduced solvent cage and seeks a more hydrated solvation state. For SO_4^{2-} ion, experiments at both the air−H_2O,[52] and CCl_4−H_2O interface indicate sulfate does alter the interfacial region, consistent with what is observed in these computations. Unlike the monovalent ions, the divalent sulfate anion has a very large first solvation shell. These calculations indicate that at the CCl_4−H_2O interface it prefers a location deeper into the aqueous phase region and affects the interface from a greater distance than the other ions. The comparison of these computations with SFG experimental results will be discussed in more detail later in the paper.

Our experimental SFG study concluded that the accumulation of the ions into the interfacial region resulted in a narrower interfacial width.[7] Our results here, based on density profile analysis, are not in agreement with the experimental conclusions. The results of simulations show that the presence of ions increases the interfacial width above that of the neat CCl_4−H_2O system. However, the relative ordering of interfacial widths respective of the anions in solution is preserved. Both studies are in agreement with NO_3^- giving rise to the smallest and SO_4^{2-} the largest interfacial width, but that of the neat CCl_4−H_2O system is different. The fitting function used here does not necessarily correspond to the interfacial cross-section detected in SFG experiments, but instead represents the molecular sharpness of the liquid−liquid transition region. SFG signals are proportional to both the number density and the orientation of molecules in an interface. Thus, the experimentally determined thicknesses will not correspond quantitatively to the simulated density profile fitting parameters but remain an informative metric for comparison.

4. Water Orientation

Previous studies have provided a detailed overview of water orientation at the interface with both air and organic phases.[4,7,9,17,28] The topmost water layers are highly disrupted because of their contact with the organic phase, and it has been suggested that ordering of both the organic and water molecules would lead to a field across the boundary of the interface.[7,9] This can influence charged species, and the ordering and orientation of the H-bond network. Our recent experimental SFG results suggest that the accumulation of charged ions leads to a field-screening that affects the orientation of waters in the topmost layers. This is complemented by the results of the current study.

The orientation of water within the aqueous/organic interface of the system was defined using the angles formed by molecular axes and the fixed reference axis of the system (perpendicular to the interfacial plane), as described previously and as depicted in Figure 1. Figure 3 shows the angle profiles of both the molecular bisector and the molecular plane normal of water molecules relative to the system reference axis at various depths into the aqueous phase. Darker red regions of the plots indicate higher orientational populations, while homogeneous coloring across the angle range indicates orientational isotropy.

In the left column of Figure 3 are the bisector orientation profiles for each of the systems. The far-left dark-blue regions of the plots show the CCl_4 bulk near the interface where few or no waters are found. The GDS is located at a depth of 0.0 Å. To the far right in the water bulk, the flat, uniformly colored profile represents the expected isotropic orientation of the bulk waters. The regions of interest lie around the GDS within the interface. The top bisector profile is that of the neat CCl_4−H_2O system, and it shows a transition in the profile beginning approximately 2 Å into the CCl_4 phase and extending up to 5 Å into the aqueous side, at which point the profile becomes orientationally isotropic. At the GDS most of the waters are oriented between $0.0 < \cos\theta < 1.0$, indicating a range of orientations as depicted in Figure 4a. In this range one of the OH-bonds points into the aqueous side, and the other straddles the interfacial plane with a slight affinity toward the organic CCl_4 phase. Just under the water surface, between 2−4 Å into the neat H_2O phase, a dark-red region spanning approximately $0.7 < \cos\theta < 1.0$ appears. This narrow orientational range is depicted in Figure 4b and is similar to the waters in the topmost aqueous layer nearer to the GDS but further limited such that one OH bond points into the H_2O side and one straddles the interfacial plane with a tendency to point into the H_2O phase.

The reference CCl_4−H_2O bisector orientational profile is comparable to previous simulations of the same system. Using slightly different simulation parameters for the same reference CCl_4−H_2O system, Wick and Dang found the free OH to point slightly into the CCl_4 phase at the GDS with an angle of $\cos(\theta_{\text{free-OH}}) \approx 0.4$.[17] This corresponds to $\cos(\theta_{\text{bisector}}) \approx 0.5$ in

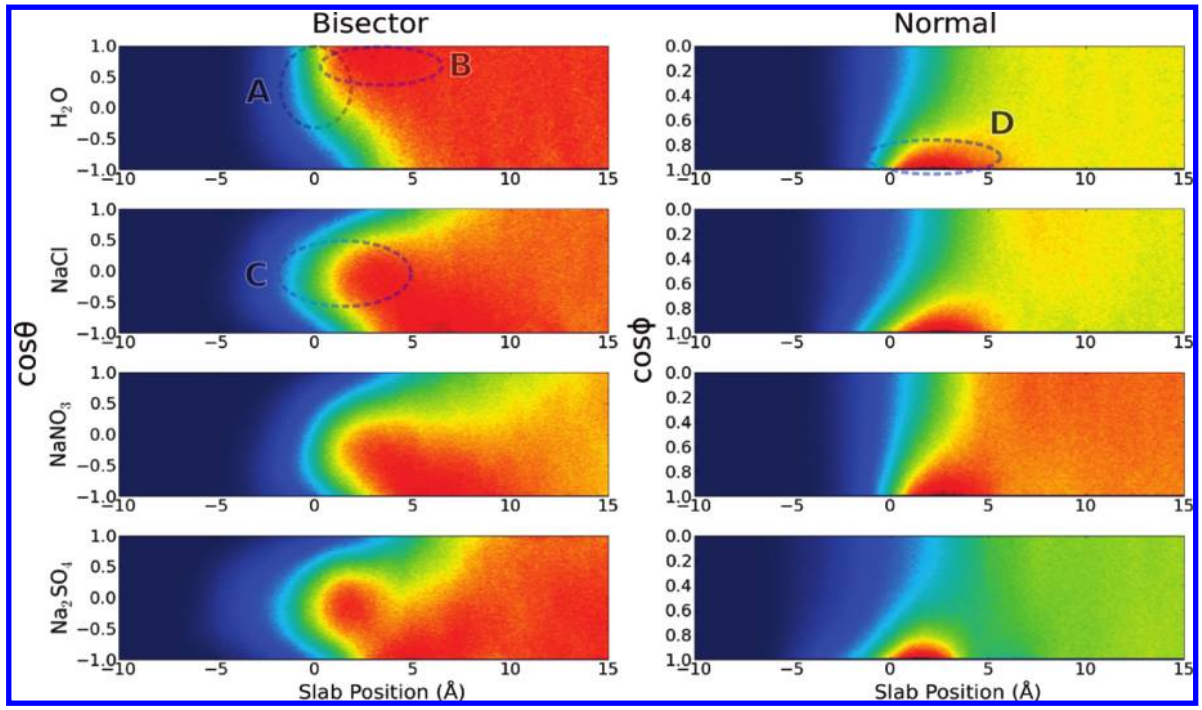

Figure 3. Orientation profiles of interfacial water molecules at different depths from the GDS. The molecular bisector profile (left column) and the profile of the molecular axis normal to the plane of the water molecule (right column) are shown. Both angle definitions are depicted in Figure 1, and the angle cosines are plotted here. The neat CCl_4-H_2O, NaCl, $NaNO_3$, and Na_2SO_4 system water orientation profiles are plotted from top to bottom, respectively. Positive position values indicate the aqueous phase, and negative positions are in the CCl_4 phase. Regions labeled in the profile correspond to orientations depicted in Figure 4.

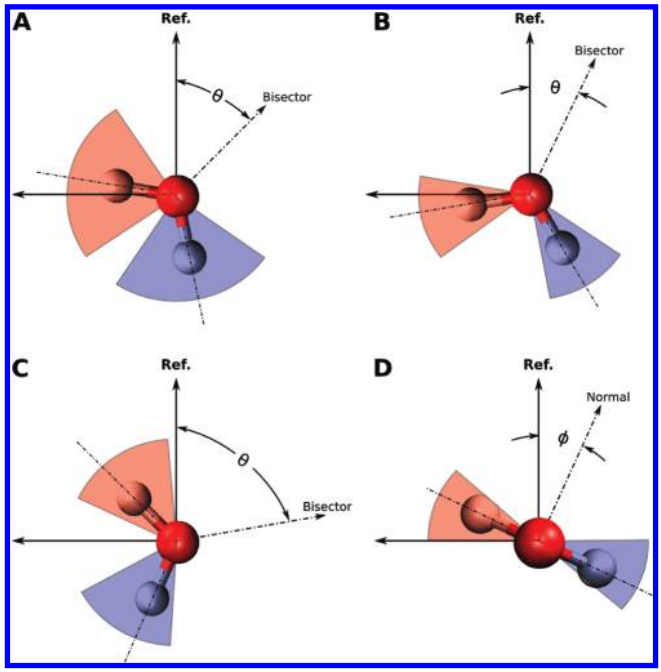

Figure 4. Depictions of water orientations spanning varying values of θ and ϕ, as defined in Figure 1. The effect of rotating the water within a fixed angle range is illustrated by the shaded (red and blue) regions that bound the OH-bonds. Ranges of θ shown here are (A) $0 < \cos\theta < 1$, (B) $0.7 < \cos\theta < 1$, (C) $-0.5 < \cos\theta < 0.5$. (D) The ϕ range of $0.7 < \cos\phi < 1$ shows the molecular plane of the water mostly flat (i.e., parallel to) the plane perpendicular to the reference axis. Depictions here correspond to those regions labeled in Figure 3.

the this work's angle definition. Similarly, deeper into the surface the angle profile diminishes such that $\cos(\theta_{free-OH}) \approx 0.0$ within 5 Å of the GDS, corresponding to $\cos(\theta_{bisector}) \approx 0.8$ in the current scheme. Those results agree with this work's reference CCl_4-H_2O profile, further complementing the experimental conclusions performed on the same systems.[7,53]

Bisector angle profiles for the salt systems show different behavior than that of the reference neat CCl_4-H_2O system. The profiles of the salt systems at the GDS all center about the cos $\theta = 0$ region, with a range of approximately $-0.5 < \cos\theta < 0.5$. This indicates a straddling water molecule with the orientational range depicted in Figure 4c. The water in that range is clearly oriented such that one OH-bond always points out of the aqueous phase into the CCl_4, and the other always points in to the water bulk. The OH-bond that would straddle the interface in the reference system points out of the interface with a greater angle. This orientation, centered at about $\cos\theta \approx 0$, extends into the water phase up to 3 Å, at which point the profile shifts to the darker region near $-1.0 < \cos\theta < 0.7$. The subsurface region of the profile between 4 and 7 Å in each system corresponds to a flip of the water orientation, as referred to in a recent SFG study as a "flip-flop" model, where water orients to counteract the field of charged species at interfaces.[54] The cation density enhancement in each salt system is within the region approximately 5−7 Å below the GDS. The waters may be orienting with the negatively charged oxygen end toward those cations and with the field established by the ion double layer within the interface. In each of the salt bisector profiles there is a clear depletion of waters oriented toward $\cos\theta = 1$, suggesting that alignment of the bisector with the reference axis is not preferred. The effect is most pronounced in the Na_2SO_4 system, where the distance between counterion density enhancements is smallest, and the transition in the bisector profile is the most abrupt, changing from a profile mostly in the range of $-1.0 < \cos\theta < 0.5$ to isotropic orientation quickly near 8 Å into the aqueous phase. The $NaNO_3$ system bisector profile shows the effect furthest into the water bulk, extending almost to 13 Å. Counterion density enhancement is most separated in $NaNO_3$, however, and most of the orientational affinity for −1.0

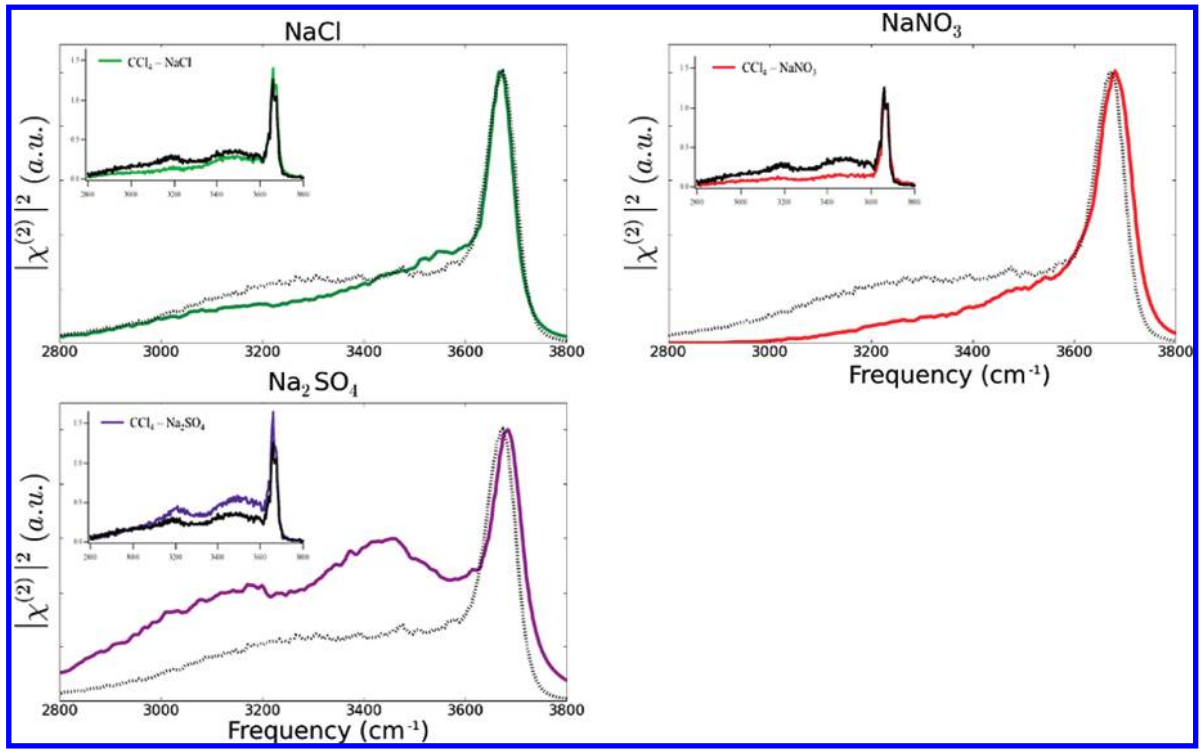

Figure 5. Vibrational SFG spectra of the water−OH stretching region for each interfacial aqueous salt−CCl_4 system. The reference CCl_4−H_2O interface spectrum (black-dashed line) is provided on each simulated SFG spectrum for reference. Insets at the top left of each spectrum are reproductions of the experimental spectra ($\chi^{(2)}_{eff}$) from McFearin et al.[7] including the reference (black) spectrum from that study. SSP polarization is used for all the spectra.

$< \cos\theta < 0.5$ occurs within the first 10 Å of the surface. The bisector profile of the NaCl system is broadest with $-1.0 < \cos\theta < 0.7$ starting near the GDS. Also, orientational isotropy is shallowest in the NaCl system starting near 7 Å into the aqueous phase.

It appears that the field established by the anion−cation pairing within the interface affects the depth to which waters are oriented before the bulk isotropic profile begins. Also, the range of orientations beneath the surface is dependent on the properties of the anion. The weakly polarizable Cl^- anion does not restrict the orientational range as much as the more polarizable NO_3^- and SO_4^{2-}. Anions also appear to control the depth to which the water orientation is felt, with the most surface-active NO_3^- anion causing the deepest effect. SO_4^{2-} anion shows the strongest restriction on the range of bisector angles and the sharpest orientational transition to the bulk, which may be attributed to the higher charge of the anion, and thus the stronger field established between the counterions in the system.

Orientational profiles for the molecular plane normal of the water molecules (ϕ-profiles) are found in the right column of Figure 3. The range of a ϕ-profile is limited to $0.0 < \cos\phi < 1.0$ because of the inherent symmetry of the plane of the water molecule. More similarity is shared between the ϕ-profiles than the bisector profiles for the different systems. The neat CCl_4−H_2O ϕ-profile is typical of the other systems in appearance, with a large clustering of water population in the range of $0.7 < \cos\phi < 1.0$ between the GDS and up to 7 Å into the aqueous phase. This particular ϕ-range is depicted in Figure 4d, showing the mostly flat (i.e., parallel to the interface) orientation of the molecular plane. It is notable that the ϕ-orientation is affected to the same depth as the first peak (dark-red region) of the bisector profile. However, in the salt systems, the second peak near to $\cos\theta = -1.0$ begins at a depth where the ϕ-profile has already become isotropic. Thus, in the salt systems, the first water layer (between the GDS and almost 4 Å into the surface) has a defined ϕ-orientation that is rather flat on the interfacial plane, but the deeper waters (4−7 Å into the interface) are isotropic in ϕ and oriented with $\cos\theta$ closer to −1.0 (an orientation with oxygen pointing into the water bulk, and hydrogens more toward the interface).

By virtue of the interdependence of θ and ϕ (the bisector is perpendicular to the molecular plane normal at all times), a value of $\cos\phi = 1.0$ implies $\cos\theta = 0$ and vice versa. However, a broad θ-range allows for a full range of ϕ-values. Although the second peak of the salt system bisector profiles is concentrated near $\cos\theta = -1.0$, the corresponding ϕ-profile is isotropic. This deeper region (the second water layer) orients with the bisector counteracting the field of the anion−cation double-layer, and the only apparent affinity is that of placing oxygen closer to the cation density enhancement (and hydrogen closer to the anion layer), while the ϕ-profile spans the entire orientational range.

5. Calculated Sum-Frequency Spectra

The effect of the varied set of anions on the CCl_4−H_2O interface is linked from simulation to empirical data through the computed SFG spectra. The computed spectra for the SSP polarization (polarization schemes are fully described in literature[55]) are presented in Figure 5 along with the experimental spectra (inserts) from our previous experimental SFG work with these same salt solutions interfaced with CCl_4.[7] Each of the spectra show a salt system response (colored traces) overlaid on the reference CCl_4−H_2O spectrum (black or dashed-black traces). On first look, the overall computed intensities and line shapes follow remarkably similar trends as in the experimental systems. All the spectra have a strong feature near 3660 cm^{-1}

coinciding with the "free OH" vibrations as defined previously[7] and corresponding to one of the uncoupled OH stretch modes from water molecules that "straddle" the interface (Figure 1a−c).[7] The broad spectral region from 3200 to 3500 cm^{-1} is attributed to the more highly coordinated OH-oscillators that are solvated at the surface or just beneath the surface with stronger hydrogen bonding. Each of the spectra computed for the salt solutions differ markedly from each other and from the neat CCl_4-H_2O spectrum. The monovalent ions (Cl^- and NO_3^-) in solution produce a measurable decrease in intensity of the lower frequencies of the spectra with very little change to the free OH mode. Like the experimental counterparts, the decrease is greatest around the 3200−3400 cm^{-1} region but shows little change from the neat CCl_4-H_2O system above 3500 cm^{-1}. As in the SFG experiment, the presence of the SO_4^{2-} anion causes an opposite effect by significantly enhancing the intensity below 3600 cm^{-1}.

The reference CCl_4-H_2O spectrum reproduces well the line shape from experiment but lacks the definition of the two peaks found near 3250 and 3450 cm^{-1}. These lower-frequency features have been attributed to the different H-bonding species of water that make up the more highly coordinated, tetrahedral environments found deeper in the interfacial region. The reference CCl_4-H_2O line shape is quite similar to that of the experiment. The salt solution spectra show an overall drop in signal when Cl^- and NO_3^- are added and an increase in intensity due to SO_4^{2-}. This suggests that the methods are sound and justified for experimental comparison in this study.

The conclusions drawn from the experiments are that the presence of anions at the interface causes a "field-screening" that decreases the innate interfacial field at the H_2O-organic interface and, consequently, the number of bonded water molecules contributing to the SFG spectrum. Both of the monovalent anions, Cl^- and NO_3^-, show this effect in their SFG spectra. For both the experiment and these calculations, comparison to the reference CCl_4-H_2O spectrum shows that the added presence of the surface-active anions decreases the lower frequency intensities. Calculations show that Cl^- affects a notably smaller decrease in the spectral intensities than the NO_3^- system, similar to experiment. This result is most likely due to the higher preference for the surface of the larger and more polarizable nitrate in the presence of CCl_4. The NO_3^- ion is extremely surface active, as seen in the density profile, and should thus cause the greatest "field-screening" to waters found deeper in the bulk.

The larger divalent SO_4^{2-} anion accumulates deeper into the aqueous bulk and exhibits the lowest surface affinity of the ions studied. This is most likely due to the higher charge of the anion that leads to greater solvation. The sulfate provides little or no screening of the interfacial field from the topmost water layer and more greatly affects the deeper, highly coordinated waters. The bonding region spanning the lower-frequency features is notably enhanced above the reference spectrum in both experiment and computation. This indicates stronger ordering of deeper interfacial waters, consistent with the anion location.

As concluded in the previous experimental work, the monovalent anions appear to screen the deeper water molecules from the field produced by the phase change at the aqueous−organic interface. This is supported by the MD simulations showing that monovalent ions show a strong surface affinity and interact with surface waters. The large but more highly charged divalent SO_4^{2-} anion experiences stronger solvation and is thus found deeper in the aqueous phase. Deeper anions do not participate as interfacial field screening agents to the same extent as their monovalent counterparts, but they act to strongly orient water near the interface, perhaps through the strong field established by the ion double layering. The distance between the counterion density peaks (Table 2) follows the inverse of the trend of SFG signal enhancement. As the ionic double layer size increases, the SFG signal decreases. Similarly, the smallest double layer size, that of the SO_4^{2-} system, produces the greatest signal enhancement across the lower frequencies of the water OH-stretching SFG spectrum. Although the water density profiles do not change markedly between the different systems, the orientational profiles do show large variation from the neat CCl_4-H_2O system and some slight variation between the salt solutions. The two factors that alter the SFG intensity are changes in the number of contributing water-bonded species and a change in orientation of various water-bonded species. From the water orientation profiles (Figure 3) it is clear that the presence of anions at the CCl_4-H_2O interface causes a strong orientation change from the reference CCl_4-H_2O system. Thus, we find that there appears to be a strong coupling between the presence and size of an ionic double layer, the subsequent reorientation of surface water molecules, and the resulting SFG signal change.

6. Conclusions

The unique environment created by interactions between water and hydrophobic molecules makes ionic adsorption and transport across interfaces possible. Aqueous−hydrophobic surfaces are of prime importance in applications ranging from ion transport, chemical remediation, and catalysis, to chemical synthesis. Complex interfaces between aqueous media and organic phases enhance chemical reactions and thus motivate research to understand such environments. This study provides an important step in understanding aqueous−organic surfaces by computationally examining simple aqueous salt solutions interfaced with hydrophobic liquid CCl_4. Through a combination of simulations and computational analysis, the nature of ionic adsorption and its effect on hydrogen bonding, geometry, and orientation of water at the liquid−liquid boundary is determined.

Analysis of the component density profiles provides a thorough microscopic picture of ionic surface affinity, double-layering, and the effect on interfacial size. The smaller and less polarizable Cl^- anion behaves at the CCl_4-H_2O surface much like at the air$-H_2O$ interface, but the larger surface-active anions do not. Density profile analysis shows that the NO_3^- anion exhibits a much greater surface affinity near the organic phase than at an air interface, consistent with experimental conclusions. The orientational analysis of the solutions shows the very different effect of the various salts on the water orientation at the CCl_4-H_2O boundary. The orientation profiles show a stratification of water geometries consistent with the emerging picture of a multilayered surface region with varied geometries and interactions. This reorientation subsequently affects the ionic double layer and subsurface waters. Such effects are manifested in spectroscopic changes to water's vibrational OH modes, as seen in both the experimental and computational results. Consequently, SFG spectra computed in this study build the necessary bridge to our previous SFG work by offering direct comparison of the computational and experimental results. The surface spectroscopic signals, measured and calculated, are altered relative to the ion-free signal, indicating a change to the water bonding at the interface due primarily to the presence of the anion. The divalent SO_4^{2-} anion acts to enhance the number and orientation of interfacial waters, while the monovalent ions have the opposite effect. Both the organic phase and

the salt anion species in solution contribute to altering the geometry of water's surface.

We have thus moved toward our goal of further understanding the behavior and impact of ions and a hydrophobic phase on water at liquid−liquid interfaces. The complementary results of both simulation and experiment have strengthened our certainty of some of the underlying surface science of these systems, but challenges still remain. A more complete picture would include knowledge of different cation effects, as well as the changes to the surface by different hydrophobic phases. The ability to analyze these important interfacial environments both theoretically and experimentally provides us with the tools to better develop our understanding of them.

Acknowledgment. The authors wish to thank the National Science Foundation (Grant CHE-0652531) and the US Department of Education Graduate Assistance in Areas of National Need (GAANN) program (Grant P200A070436) for support of this research.

Supporting Information Available: The results of calculations and analyses that support this work and analyses of electric field and the $\chi^{(2)}$ spectra that were auxiliary to the results included in the paper. This material is available free of charge via the Internet at http://pubs.acs.org.

References and Notes

(1) Charreteur, K.; Quentel, F.; Elleouet, C.; L'Her, M. *Anal. Chem.* **2008**, *80*, 5065–5070.
(2) Chen, X.; Yang, T.; Kataoka, S.; Cremer, P. S. *J. Am. Chem. Soc.* **2007**, *129*, 12272–12279.
(3) Luo, G.; Malkova, S.; Yoon, J.; Schultz, D.; Lin, B.; Meron, M.; Benjamin, I.; Vanysek, P.; Schlossman, M. *Science* **2006**, *311*, 216–218.
(4) Wick, C. D.; Dang, L. X. *Chem. Phys. Lett.* **2008**, *458*, 1–5.
(5) Schnell, B.; Schurhammer, R.; Wipff, G. *J. Phys. Chem. B* **2004**, *108*, 2285–2294.
(6) Wardle, K.; Henderson, D.; Rowley, R. *Fluid Phase Equilib.* **2005**, *233*, 96–102.
(7) McFearin, C. L.; Richmond, G. L. *J. Phys. Chem. C* **2009**, *113*, 21162–21168.
(8) Hore, D. K.; Walker, D. S.; MacKinnon, L.; Richmond, G. L. *J. Phys. Chem. C* **2007**, *111*, 8832–8842.
(9) Hore, D. K.; Walker, D. S.; Richmond, G. L. *J. Am. Chem. Soc.* **2008**, *130*, 1800+.
(10) Hore, D. K.; Walker, D. S.; Richmond, G. L. *J. Am. Chem. Soc.* **2007**, *129*, 752–753.
(11) Walker, D. S.; Hore, D. K.; Richmond, G. L. *J. Phys. Chem. B* **2006**, *110*, 20451–20459.
(12) Walker, D. S.; Richmond, G. L. *J. Am. Chem. Soc.* **2007**, *129*, 9446–9451.
(13) Walker, D. S.; Moore, F. G.; Richmond, G. L. *J. Phys. Chem. C* **2007**, *111*, 6103–6112.
(14) Chang, T.; Peterson, K.; Dang, L. *J. Chem. Phys.* **1995**, *103*, 7502–7513.
(15) Eggimann, B. L.; Siepmann, J. I. *J. Phys. Chem. C* **2008**, *112*, 210–218.
(16) Du, H.; Liu, J.; Ozdemir, O.; Nguyen, A. V.; Miller, J. D. *J. Colloid Interface Sci.* **2008**, *318*, 271–277.
(17) Wick, C.; Dang, L. *J. Phys. Chem. B* **2006**, *110*, 6824–6831.
(18) Petersen, P.; Saykally, R.; Mucha, M.; Jungwirth, P. *J. Phys. Chem. B* **2005**, *109*, 10915–10921.
(19) Matsumoto, M.; Kataoka, Y. *J. Chem. Phys.* **1988**, *88*, 3233–3245.
(20) Petersen, P.; Saykally, R. *Annu. Rev. Phys. Chem.* **2006**, *57*, 333–364.
(21) Allen, H. C.; Casillas-Ituarte, N. N.; Sierra-Hernandez, M. R.; Chen, X.; Tang, C. Y. *Phys. Chem. Chem. Phys.* **2009**, *11*, 5538–5549.
(22) Hofft, O.; Borodin, A.; Kahnert, U.; Kempter, V.; Dang, L.; Jungwirth, P. *J. Phys. Chem. B* **2006**, *110*, 11971–11976.
(23) Beattie, J.; Djerdjev, A.; Franks, G.; Warr, G. *J. Phys. Chem. B* **2005**, *109*, 15675–15676.
(24) Bian, H.-t.; Feng, R.-r.; Guo, Y.; Wang, H.-f. *J. Chem. Phys.* **2009**, *130*.
(25) Dang, L. *Abstr. Pap.—Am. Chem. Soc.* **2004**, *228*, 86–PHYS.
(26) Thomas, J. L.; Roeselova, M.; Dang, L. X.; Tobias, D. J. *J. Phys. Chem. A* **2007**, *111* (16), 3091–3098.
(27) Wick, C. D.; Kuo, I.-F. W.; Mundy, C. J.; Dang, L. X. *J. Chem. Theory Comput.* **2007**, *3*, 2002–2010.
(28) Fan, Y.; Chen, X.; Yang, L.; Cremer, P. S.; Gao, Y. Q. *J. Phys. Chem. B* **2009**, *113*, 11672–11679.
(29) Galamba, N.; Cabral, B. J. C. *J. Am. Chem. Soc.* **2008**, *130*, 17955–17960.
(30) Ishiyama, T.; Morita, A. *J. Phys. Chem. C* **2007**, *111*, 738–748.
(31) Morita, A.; Hynes, J. *Chem. Phys.* **2000**, *258*, 371–390.
(32) Walker, D. S.; Richmond, G. L. *J. Phys. Chem. C* **2008**, *112*, 201–209.
(33) Morita, A.; Hynes, J. *J. Phys. Chem. B* **2002**, *106*, 673–685.
(34) Ishiyama, T.; Morita, A. *J. Phys. Chem. C* **2009**, *113*, 16299–16302.
(35) Chang, T.; Dang, L. *J. Phys. Chem. B* **1997**, *101*, 10518–10526.
(36) Dang, L. *J. Phys. Chem. B* **1999**, *103*, 8195–8200.
(37) Hrobarik, T.; Vrbka, L.; Jungwirth, P. *Biophys. Chem.* **2006**, *124*, 238–242.
(38) Caldwell, J. W.; Kollman, P. A. *J. Phys. Chem.* **1995**, *99*, 6208–6219.
(39) Rivera, J. L.; Starr, F. W.; Paricaud, P.; Cummings, P. T. *J. Chem. Phys.* **2006**, *125*.
(40) Petersen, P.; Saykally, R. *J. Am. Chem. Soc.* **2005**, *127*, 15446–15452.
(41) Dang, L. *J. Phys. Chem. B* **1998**, *102*, 620–624.
(42) Salvador, P.; Curtis, J. E.; Tobias, D. J.; Jungwirth, P. *Phys. Chem. Chem. Phys.* **2003**, *5*, 3752–3757.
(43) Chang, T.; Dang, L. *J. Chem. Phys.* **1996**, *104*, 6772–6783.
(44) Wick, C.; Dang, L. X. *J. Chem. Phys.* **2007**, *126*, 134702.
(45) Jungwirth, P.; Tobias, D. *Chem. Rev.* **2006**, *106*, 1259–1281.
(46) Wick, C.; Dang, L. *J. Phys. Chem. B* **2006**, *110*, 8917–8920.
(47) Miller, Y.; Thomas, J. L.; Kemp, D. D.; Finlayson-Pitts, B. J.; Gordon, M. S.; Tobias, D. J.; Gerber, R. B. *J. Phys. Chem. A* **2009**, *113*, 12805–12814.
(48) Otten, D. E.; Petersen, P. B.; Saykally, R. J. *Chem. Phys. Lett.* **2007**, *449*, 261–265.
(49) Xu, M.; Tang, C. Y.; Jubb, A. M.; Chen, X.; Allen, H. C. *J. Phys. Chem. C* **2009**, *113*, 2082–2087.
(50) Schnitzer, C.; Baldelli, S.; Shultz, M. *J. Phys. Chem. B* **2000**, *104*, 585–590.
(51) Brown, M. A.; Winter, B.; Faubel, M.; Hemminger, J. C. *J. Am. Chem. Soc.* **2009**, *131*, 8354.
(52) Gopalakrishnan, S.; Jungwirth, P.; Tobias, D.; Allen, H. *J. Phys. Chem. B* **2005**, *109*, 8861–8872.
(53) Scatena, L.; Richmond, G. *J. Phys. Chem. B* **2001**, *105*, 11240–11250.
(54) Nihonyanagi, S.; Yamaguchi, S.; Tahara, T. *J. Chem. Phys.* **2009**, *130*.
(55) Lambert, A.; Davies, P.; Neivandt, D. *Appl. Spectrosc. Rev.* **2005**, *40*, 103–145.

JP1023668